ÉCOLE POLYTECHNIQUE FÉDÉRALE DE LAUSANNE

MONITORING EVAPOTRANSPIRATION CHANGES IN A VEGETATED SOIL

MASTER THESIS

Simon Burkhardt

Project advisor : Prof. Andreas Rinaldo

Co-advisor : Dr. Paolo Benettin

30th June 2022

ABSTRACT

Evapotranspiration (ET) is one of the main fluxes of the water cycle and is a fundamental driver of complex processes intertwined between the fields of hydrology and ecology. Widespread models using a constant water availability factor ($K = ET_a/ET_{potential}$) are consistent for a balanced soil moisture, but are unable to account for the processes occurring in stress conditions. Further understanding of these mechanisms requires accurate ET measurement that can be achieved with lysimeters.

This master project intends to answer the following questions : 1) What is the effect of soil vegetation cover on water evapotranspiration ? 2) How does the lack of precipitation (drought) affect the transpiration of vegetation ? A monitoring experiment provided a data set of ET, soil moisture and water tension of three grass vegetated and one bare soil lysimeters and the meteorological context to support this reflection. On one hand, the results showed that vegetation significantly increased the water availability as it confined water at root depth and increased the water withdrawal limit. As a result, grass cover approximately doubled the mean ET rate. On the other hand, droughts force vegetation to apply a greater root suction such that water leakage approaches zero. Vegetation wilting due to extended exposure to stress conditions results in long term drifts and feedback patterns of the transpiration ability of vegetation.

To my grandfather Ernest Burkhardt

I cannot begin to express my thanks to Dr. Paolo Benettin, who accompanied me along every step of this project and gave me his trust. I also would like to extend my sincere thanks to Pr. Andrea Rinaldo for making this project possible and for his support. Finally, I'm extremely grateful to PhD Concetta D'Amato for her help and support with the difficulties encountered and her incredible enthusiasm.

Contents

CHAPTER 1

INTRODUCTION

1.1 CONTEXT

The field of ecohydrology is reasonably young in the sense that it follows the needs of exploring interactions between hydrology and ecological patterns. Landscape water cycle is typically a fundamental driver of ecological patterns that has itself long term feedback on the distribution of large scale water fluxes. Closing the water balance is one of the main challenges faced in many landscape studies and has tremendous implications for soil ecology (Benettin et al. 2021, P. Queloz et al. 2015). In landscape hydrology, evapotranspiration is one of the main flux of water cycle and is closely related to the heat balance. This typically accounts for 40% of precipitations and 38% of solar radiation absorbed by the soil (Fatichi, Pappas and Ivanov 2016). Furthermore, the process induced by vegetation is tightly related to water availability at root level (Fatichi, Pappas and Ivanov 2016).

1.2 MOTIVATION

Many applications in the field of ecohydrology rely on the ability to estimate the evapotranspiration flux rate and temporal distribution. A widespread model consists in computing the actual ET (ET_a) from potential ET ($ET_{potential}$) using a constant water availability factor ($K = ET_a$). Typically, estimations of $ET_{potential}$ are derived from the energy balance between atmospheric conditions and soil heat flux. Such methods are commonly used for hydrological engineering estimation at short term. However, water cycle and vegetation feedback along with the vegetation dynamics in specific conditions, such as water stress, have fundamental implications in land-surface climate and carbon cycles or long term studies (Fatichi, Pappas and Ivanov 2016). In this context, the importance of vegetation dynamic response to its environment motivates the needs of higher complexity models. The development of such tools suffers from a clear lack of data to relate soil physics descriptive variables with precise ET measurements. The major limitation follows that no method provides accurate estimations of ET in landscape. Nevertheless, continuous and accurate ET rate measurement can be easily estimated using lysimeters. Lysimeters consist in open tanks that contains a specific soil column exposed to natural precipitations and atmospheric conditions. The container top matches the natural ground surface and an underground control room allows to access the sides and the bottom. The tank is placed on highly responsive weight sensors. As water evaporates from the soil, the total weight of the column reduces accordingly to the lost water volume. Moreover, such devices facilitate the installation of various soil sensors to explore soil water physics variables and their implication in ET process.

1.3 GOALS

The purpose of this master thesis is to monitor ET and water availability in vegetated lysimeter in normal and stress conditions. In particular, the project aims to address the following research questions : 1) What is the effect of soil vegetation cover on water evapotranspiration ? 2) How does the lack of precipitation (drought) affect the transpiration of vegetation ? The following report first focuses on the methods used to monitor soil and environmental variables and the required processes to estimate ET rate from outdoor lysimeters. Primary data analysis is furthermore provided as an attempt to highlight dynamics between ET and water availability.

CHAPTER 2

METHODS

2.1 EXPERIMENTAL DESIGN

2.1.1 EXPERIMENT TIMELINE

This project relies on two experiments that aim to characterise evapotranspiration (ET) in vegetated lysimeters in distinct environmental conditions. The first experiment runs from the 5^{th} of April to the 8^{th} of May and consists in measuring ET rate under natural atmospheric condition. The conditions were homogeneous for all lysimeters to provide a redundant set of measurements and highlight variability of the ET processes. The second experiment runs from the 9^{th} of May to the 8^{th} of June and focuses on the effect of draught on ET rate. The manipulation of water input using shelters and manual irrigation allows to induce stress conditions for vegetation and observe shifts in water behaviour pattern. We irrigated the lysimeters unevenly to obtain a gradient of stress conditions and explore the non-linearity of ET in a scarce water context (WC). The rapid growth of the lawn required mowing on the 13^{th} of April. At the end of the first experiment, L1 and L3 reached about 30 cm height and L6 up to 50 cm. For better homogeneity, measurement of the second experiment starts after a second grass cut on the 9^{th} of May. Irrigation on the 18^{th} and the 24^{th} of May prevented the grass from complete dry out to carry out the monitoring.

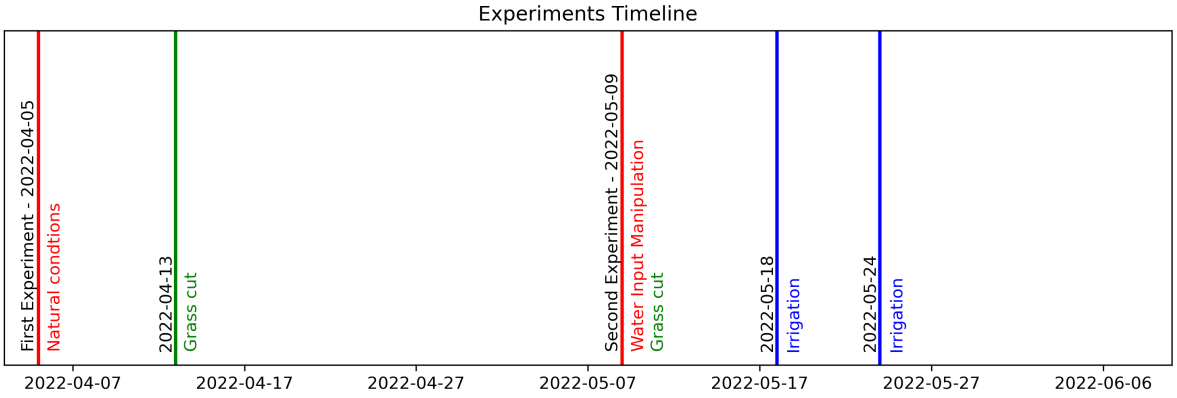

Figure 2.1: Summary of experiment phases and noticeable interventions.

2.1.2 EQUIPMENT DESCRIPTION

The outdoor lysimeters used to conduct this study are located in a meadow on the EPFL campus. The vegetated area is surrounded by 3-4 floor buildings but with limited effect of shadowing for the measurement period.

Three lysimeters were vegetated with precultivated grass as duplicate to improve the resilience of the system and allow to capture the variability of ecohydrologic processes. An additional lysimeter with bare soil is used as control.

Each lysimeters rests on analogic load cells (RTNC3/2.2T, HBM, Germany) connected to a junction box (Fig. A.1a, VKK1-4, HBM). The signal is then converted using an analogic-digital transducer (Fig. A.1b, AED9201B, HBM). The output generated is added to the next transducer that collects the measurements of an additional lysimeter load cell set. As depicted on figure 2.3, one 15 volts DC powers each group of two transducers. The terminal transducer "Addr1" in fig.2.3 is connected to a computer through an interface converter RS-232 (SC232/422B, HBM) (P. C. J. Queloz 2015). Dedicated software provided by HBM (AED_Panel32) is used to record the absolute weight value of the soil column every 20s. We provided basic repairs and maintenance to the equipment accordingly to the needs of this project.

Figure 2.2: Context of the lysimeter installations

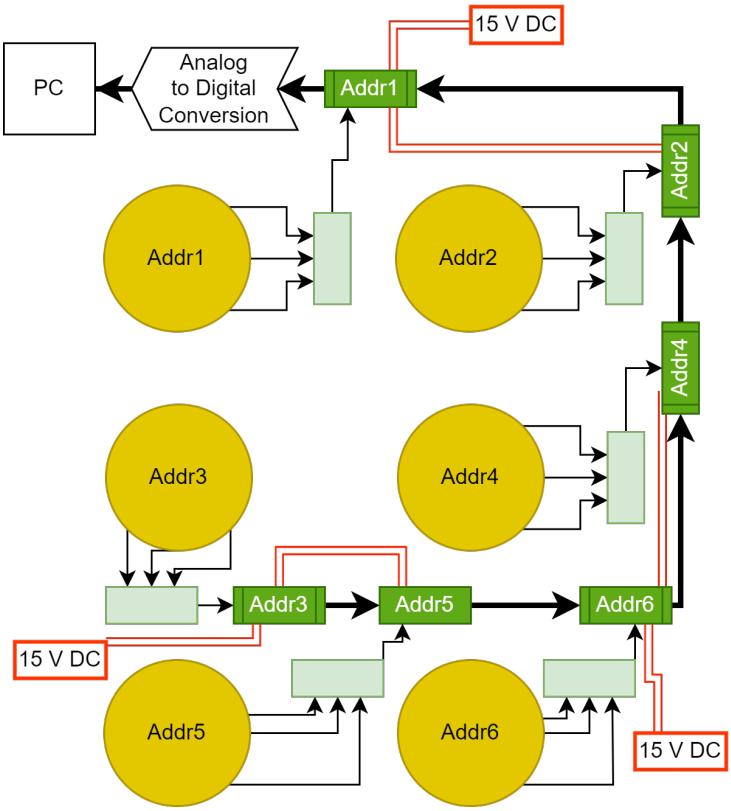

Figure 2.3: Schematic of weight sensor network

2.1.3 ATMOSPHERIC DATA

A weather station (MeteoMADD, MADD Technologies Sàrl, Switzerland) installed at 5 meters from the lysimeters provided solar radiation, air temperature, humidity, wind speed and pluviometry (tipping bucket) measurement every 15 minutes.

2.1.4 REFURBISHMENT OF LYSIMETERS

The lysimeters had remained unused for several years, before the present experiments. To protect the installation when not used, opaque shields cover the visible part and prevent both light and precipitation incomes. Consequently, the previous vegetation and soil had dry out and formed a gap of few centimeters at the borders of the tanks (figure 2.4a). Such conditions require intensive irrigation to allow manual plowing. We entirely removed remains of vegetation and pruned surrounding higher grass and willows to avoid shading effects. We filled the tanks up to 2cm from their edge to limit water pounding and hot surface radiation effect of the walls (figure 2.4b). The added soil comes either from unused lysimeters or a nearby pile. Finally, we installed pre-cultivated grass carpets on lysimeters (L6, L3, L1). As advised by the supplier, we removed large rocks at ground surface to increase the attachment of the carpet (figure 2.4c).

(a) Dry vegetation and compacted soil

(b) Soil fill and surface preparation

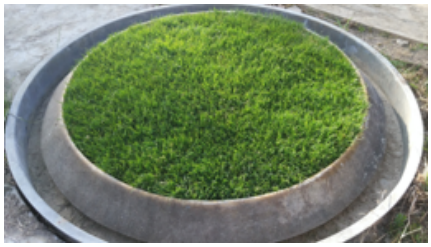

(c) Vegetated lysimeters at the beginning of measurements

Figure 2.4: Lysimeter vegetation refurbishment

2.1.5 GRASS INSTALLATION PROTOCOL

We used six rolls of pre-cultivated grass ($4m^2$) to cover all three lysimeters. The lawn farm of *Burdet Gilles* (Mathod, Switzerland) was able to supply such a small quantity. The installation pattern of the grass rolls is constant to ensure homogeneity of grass density between lysimeters. We slightly oversized the grass carpet to induce horizontal pressure and improve junction sealing.

2.2 SENSOR NETWORK

Two independent sensor networks for lysimeters L6, L4 and L3, L1 monitor water content and matric potential. Such division allows to efficiently reduce the wiring length and increase robustness of the system. Each network is autonomous and only requires punctual battery replacement.

Figure 2.5: Data network box

Programmable Campbell scientific® dataloggers (CR800 or CR1000) carry the measurement routine. Each network collects measurements from 12 Decagon 5TM water content probes and 4 Meter TEROS 21 tensiometers. Both sensors are compatible with SDI-12 protocol for communication with non-Meter datalogger and allow to be managed through the same bus connection. A single communication port on a

CR1000/800 supports up to 16 digital sensors using a SDI-12 protocol which is sufficient for the present application.

Bus connection consists in linking sensors in parallel and allows to transmit signal from multiple digital sources through one single channel. Figure 2.6 shows the interior of the junction box build for this experiment. It features 17 3.5 mm female jacks compatible with the serial plug of the sensors shown in figure **??**. The wiring connects and groups down each type of terminal (ground, digital communication, power) to a single female 3.5mm stereo plug that links the datalogger. They both feature the following port labeling : "G" for ground, "SW12" for switch 12V and "C1" of communication port n°1. The SDI-12 protocol used in bus connection is highly sensitive to sensor failure as the measurement routine stops if one single sensor disconnects. For higher system resilience and easier visual check-up, all wires were directly welded to plug electrical strips.

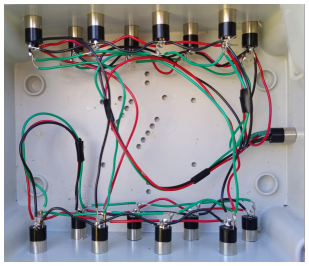

Figure 2.6: Interior of a derivation box

Rechargeable lead acid 12 volts batteries provides power supply and require regular check. We replaced one battery after only three weeks as the network drained abnormally great amount of power.

2.2.1 SOIL SENSORS

Figure 2.7: 5TM water content probe

This experiment relies on water content and water tension monitoring to estimate water availability. 5TM from Decagon provides an estimation of water content by measuring dielectric permittivity. The probe sprung use an oscillating current at 70Mhz that generated an electric field. The accumulated charge measured depends on the dielectric permittivity of the surrounding soil which heavily depends on water content.
The Topp transfer equation (Topp, Davis and Annan 1980) converts the dielectric permittivity to volumetric water content :

$$VWC = 4.3 * 10^{-6}\epsilon_a^3 - 5.5 * 10^{-4}\epsilon_a^2 + 2.92 * 10^{-2}\epsilon_a - 5.3 * 10^{-2} \quad (2.1)$$

TEROS 21 from METER reflects water tension dynamics thanks to a measure of matric potential. The sensor is composed by a moisture probe between two ceramic discs. The sensor measures the water content of the discs and computes the matric potential as their ability to draw water from the soil depending on their pore size distribution and the water potential of the soil. The pore size distribution is known and allows calibration by the manufacturer.

2.2.2 DATALOGGER CONFIGURATION AND MANAGEMENT

Campbell Scientific provides PC400 software for free that allows to connect and configure any of their datalogger and download records. The devices communicate through a RS-232 port and require an usb conversion interface to link with a computer. The first step was to upload a CRBasic scripts to pilot the measurement routine on the CR1000 and CR800. Thankfully, Campbell Scientific provides 5TM configuration template for both dataloggers Colin Campbell 2016. High frequency sensors scan script results in data loss due to many skipped measurement and slow scans. A 5 minutes interval avoided this issue and provided dense measuring points for consistent lower frequency conversion. PC400 also features a status monitor that displays numerous informations such as recorded measurements issues, power supply voltage and internal battery condition.

Figure 2.8: TEROS 21 Tensiometer

2.2.3 SOIL SENSOR INSTALLATION

Water availability depends on the soil structure such as preferential path and grain size distribution as they are main drivers of water content and tension distribution across the soil column. This factors typically have a high spacial heterogeneity and their mean behavior is complex to measure. To capture this variability and provide more representative measurements, we installed three WC probes per depth in each lysimeter. We placed tensiometers in trenches "A" with a angle of 90° w.r.t. WC sensors to avoid the need of digging a fourth trench, which is a highly destructive process. The distribution of sensors is summarised in table 2.1.

Table 2.1: Summary of lysimeters

Lysimeter	Cover	Soil depth [cm]	Sensor depths [cm]	Datalogger	Weight sensor ID
L6	Grass	50	10, 35	CR800	ADR6
L4	Bare soil	40	10, 30	CR800	ADR4
L3	Grass	100	10, 35	CR1000	ADR3
L1	Grass	100	10, 35	CR1000	ADR1

For this expermient, we measured water content and matric potential at 10 cm and 35cm depth, excepted for L4 where sensor are at 10 cm and 30 cm due to shallower soil. Figure A.3 shows the trenches excavated during sensor installation.

We established a consistent protocol during this phase to ensure homogeneity between lysimeters, minimize the impact on grass cover continuity, optimize sensor placement for representative measurements, reduce artificial preferential path and protect sensor's integrity.

The protocol detailed photographs are in appendix A.3 and is as follow :

- Cut grass layer and shallow roots in a circle of 10-15 cm diameter with a knife and remove the grass clod in one piece.
- Excavate a narrow trench down to 40 cm deep with an auger, then enlarge the bottom with a hand shovel such that WC could be inserted horizontally.
- Refill the trench by adding alternatively few centimeters of soil and some water.

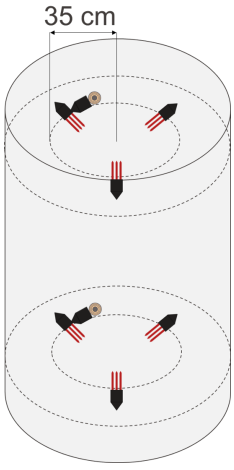

Figure 2.9: Sensor distribution in soil column

- Apply light pressure regularly to pack the soil close to bulk density, while preventing damage on sensors.
- For the TEROS 21, compact a mixture of water and soil around the ceramic to ensure a proper joining within the installation slit as the shape of tensiometers do not allow to insert them directly into the soil.
- Finally, carefully replace the block of grass at the end of the installation to limit the damage caused by digging manipulation on vegetation continuity.

2.3 COMPUTING ET IN WEIGHED LYSIMETERS

2.3.1 WATER BALANCE EQUATION

In this experiment, we model lysimeters as water tanks with the total weight of the soil column equal to the sum of the total soil and water weights, namely :

$$W = S + W_s \Leftrightarrow \frac{dW}{dt} = \frac{dS}{dt} + \frac{dW_s}{dt} = \frac{dS}{dt} \tag{2.2}$$

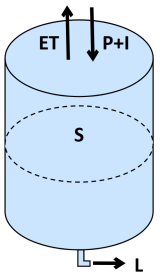

Figure 2.10: Water fluxes model of a lysimeter

For the further computation, we assume that biomass and soil mass variations are negligible such that weight is only driven by precipitation and irrigation (inputs) and evapotranspiration (output). The general mass balance of a lysimeter is then as follows :

$$\frac{dW}{dt} = P + I - ET - L \tag{2.3}$$

The lower part of lysimeters features enough free space to avoid artificial water head building up in the soil column. Evapotranspiration is then :

$$ET = \frac{dW}{dt} - (P + I) \tag{2.4}$$

2.3.2 RAIN DETECTION ALGORITHM

Without considering external perturbations and sensor drift, weight variations are mainly driven by precipitation and evapotranspiration. Moreover, due to cloudy condition and air humidity saturation, ET becomes negligible w.r.t. precipitation during rain event. From these observations, the following can be stated :

$$f(x) = \begin{cases} P(t) = \frac{dW}{dt}, & \text{if } \frac{dW}{dt} > 0 \\ ET(t) = \frac{dW}{dt}, & \text{otherwise} \end{cases} \tag{2.5}$$

Despite the heavy filtering procedure applied to obtain the weight derivative, positive values are regularly generated in dry conditions during night time when the evapotranspiration is close to zero. Therefor, a rain event detection algorithm was necessary to compute the precise precipitation received by each lysimeter. The weight value for a given time step is compared to the mean of the weight value of the four following time steps. If the increase is great enough, the time step is saved and the next one is evaluated. This can be summarised from equation 2.5 as follows :

$$f(x) = \begin{cases} P[t_i] = \frac{dW}{dt}[t_i], & \text{if } \sum_{n=t_i+1}^{t_i+5} W[n] > W[t_i] + \textit{threshold} \\ P[t_i] = 0, & \text{otherwise} \end{cases} \tag{2.6}$$

The value of the threshold in equation 2.6 has a major impact on the accuracy of the detection. Reference precipitation measurements from the weather station allow to perform a calibration of this parameter using the cumulative precipitation.

$$P_{ref}^{cum} \approx P^{cum}(threshold) \tag{2.7}$$

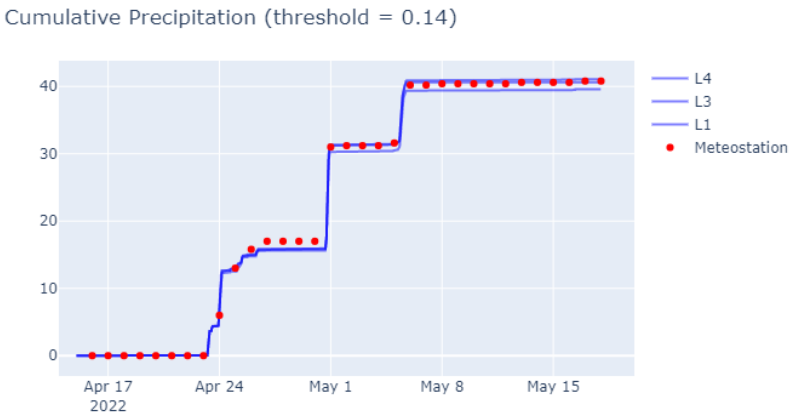

Figure 2.11: Comparison between the cumulative precipitations recorded by the MeteoMADD station and computed from the weight derivative of L1, L3 and L4. Noise of L6 generated an incoherent result and was removed from the calibration.

The threshold of 0.14 allowed to measure very similar cumulative precipitations than the tipping bucket and efficiently avoided to be triggered by noise.

2.4 DATA MANAGEMENT

2.4.1 SIGNAL FILTERING PROCESS

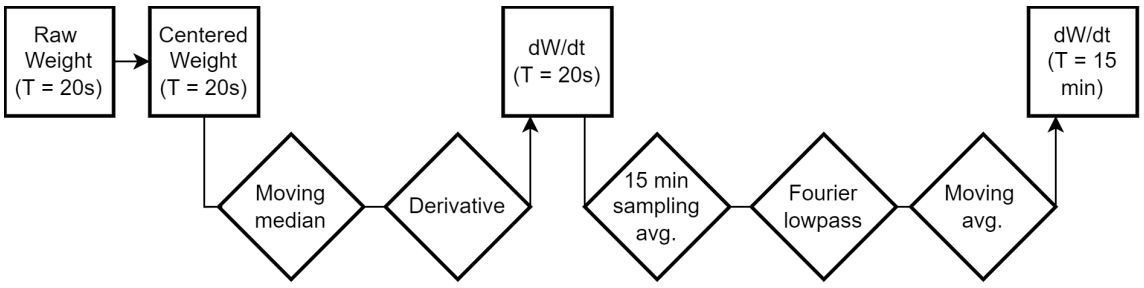

Figure 2.12: Signal processing steps for weight data

Weight monitoring software records value every 20 seconds in kilograms using a two decimal format, namely 10 grams precision. The noise-signal ratio only allows visual appreciation of weight variation and must be filtered for derivative analysis. We wrote a python script to conduct the following computations. Firstly, a moving median with a 15 min width window smooths out the high frequency variations and excludes localised peaks. Secondly, a discrete first order derivation algorithm computes $\frac{\Delta W}{\Delta t}$ for $t = 20s$. Then, we aggregate measurements every 15 minutes with their average value. Finally, a Fourier low-pass and a moving average bring out the daily ET patterns that are considered in the present report.

2.4.2 SHELTERING

The water input control experiment requires a way to prevent natural precipitation entering the lysimeters. The shelters need to have as little impact on other variables as possible. The final design features three thin transparent PVC sheets joined in a curve shape that have minimal impact on solar radiations, while efficiently evacuating water. The cover reaches 50 cm above the ground and is slightly larger than the lysimeters to limit lateral exposure to precipitation and leaves room for the grass growth. The openings on the also provide natural ventilation and limit the accumulation of hot air. Four tent pegs allow to stabilise the structure and reduce the wood joist size structure to prevent shading effect. Transparent tape ensures the sealing between the sheets and increases the general steadiness.

Figure 2.13: Rain shelter on L6. Extended drought lead a complete dry out of the grass.

2.4.3 IRRIGATION PROCESS

The dry and hot period following the second grass cut resulted in the complete dry out of an important portion of the grass. Therefore, we decided to apply irrigation to carry out the measurements in vegetated conditions.

Both irrigation process targeted water inputs of 10 liters for L6 and 20 liters for L3 and L4, while limiting the input rate to 20 mm/h to avoid ponding. For convenience, we used a dripping system with a sufficiently small supply flow. However, the bare soil permeability is very low and water tends to accumulate despite these precautions. Vegetated lysimeters absorb more easily the water and punctual addition of water using a watering can speed up the process.

Figure 2.14: Yellowing of vegetation after two weeks of exposure to hot and dry outdoor weather following the grass cut.

CHAPTER 3

RESULTS

3.1 METEOROLOGICAL DATA

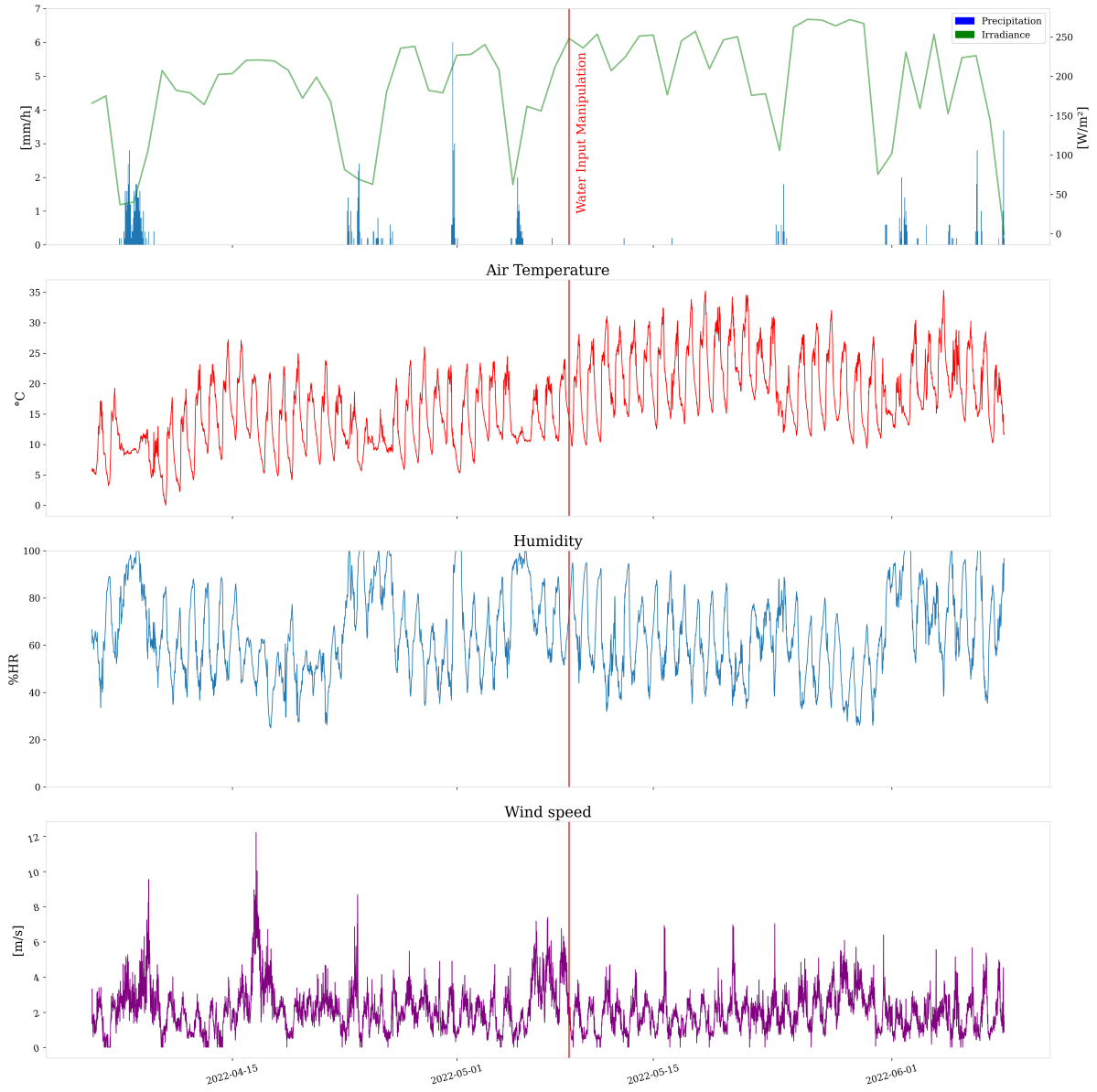

Figure 3.1: Meteorologic context of experiments

The project took place from the 5^{th} of April to the 8^{th} of June. The shift of atmospheric conditions along the measurements period clearly reflects the seasonal change from spring to summer. Generally scarce precipitations from the end of April to June follow a single intense event (40mm) between the 7^{th} and the 8^{th} of April.
During the first experiment mean values of daily precipitation, solar radiation, wind velocity and air temperature are respectively 2.4 mm/h, 170.5 W/m^2, 65.5 %RH, 13.2°C. The second experiment started with a 2 weeks drought period in summery conditions with mean atmospheric conditions to respectively 1.0 mm/h, 212.8 W/m^2, 64.7 %RH, 20.4°C.

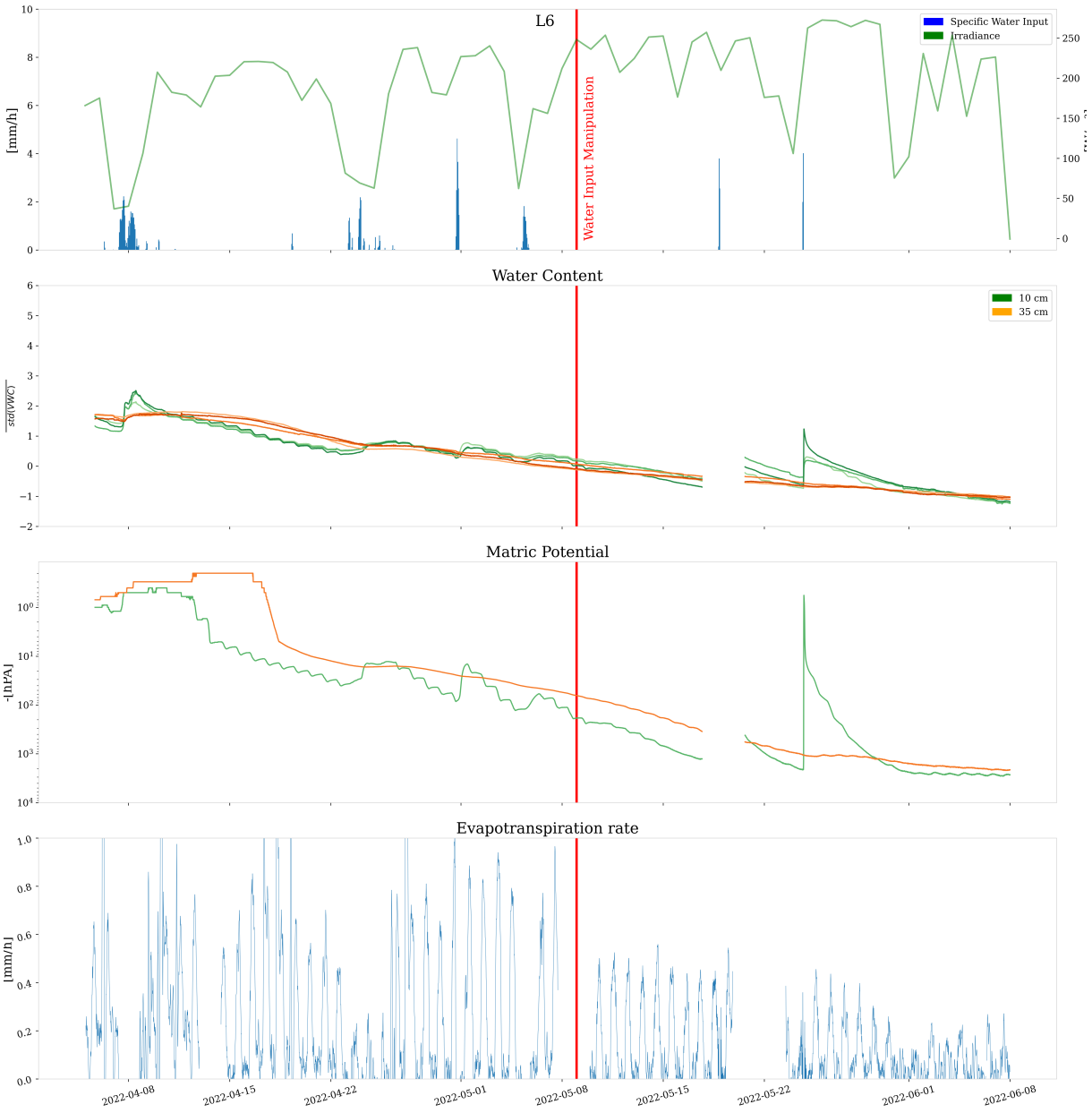

Figure 3.2: Summary of data for L6

3.2 DATA FOR EACH LYSIMETER

L6 weight measurements are affected by a significant noise which can lead to over estimations of instantaneous evapotranspiration and precipitation. Mean daily ET during the first experiment was 7.1 mm/d with a mean precipitation value of 2.8 mm/d. During the second part of the experiment, L6 sheltering, irrigation and grass cut resulted in a decrease of mean daily ET to 2.7 mm/d and mean water supply to 0.5 mm/d. Moreover, figure 3.2 shows a stabilisation of WC and water tension in the 35 cm layer.

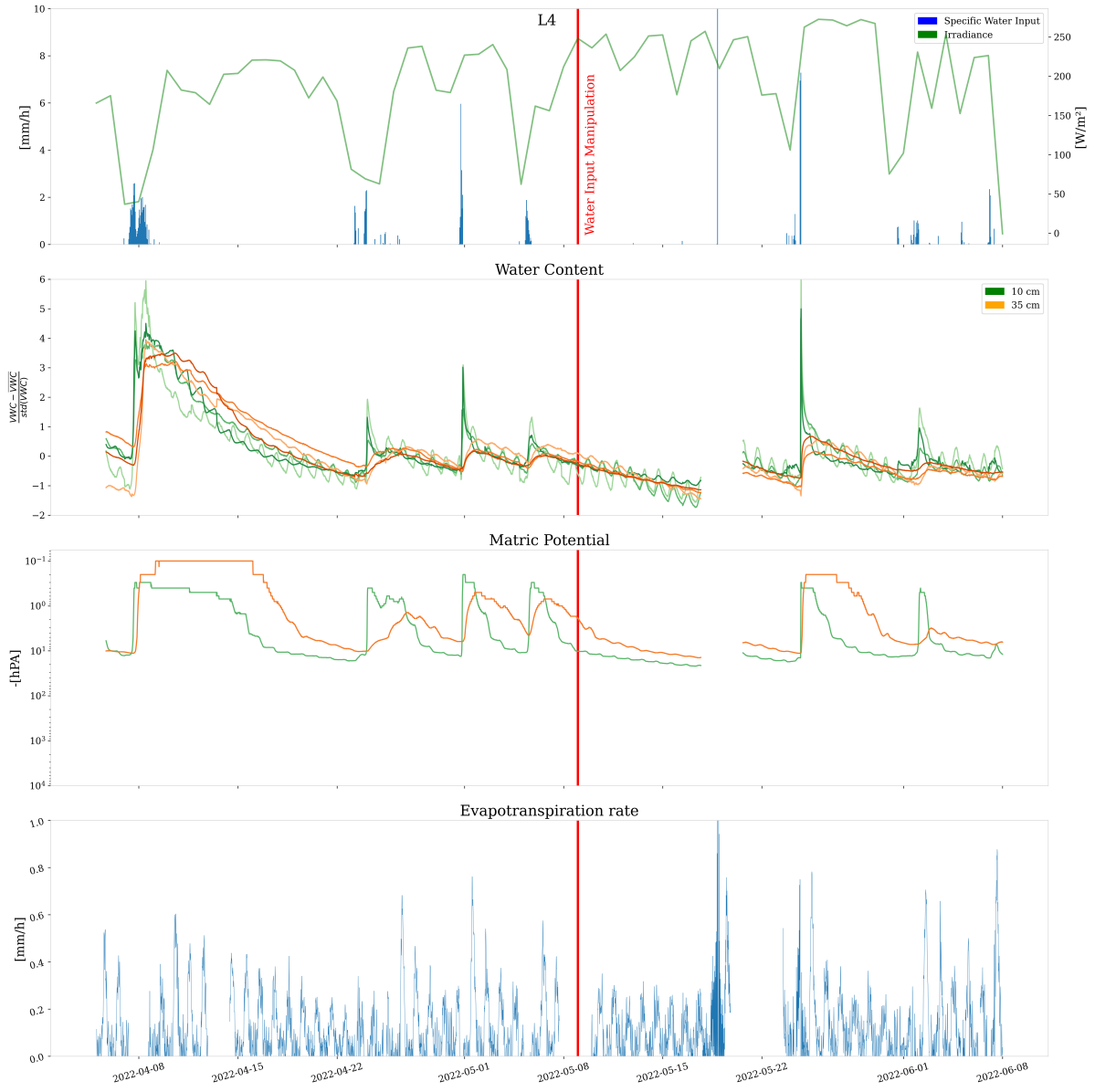

Figure 3.3: Summary of data for L4

L4 is a bare soil control lysimeter. Measured mean daily ET during the first experiment was 2.8 mm/d with a mean precipitation of 2.9 mm/d. Over the first week, the top layer WC decreased by a factor 4 before stabilising. Figure 3.3 highlights the fast response of WC and matric potential during intense precipitation events and punctual irrigations. During the second part of the experiment, irrigation and grass cut resulted in a decrease of mean daily ET to 2.8 mm/d and mean water supply to 1.8 mm/d.

Measured mean daily ET during the first experiment for L3 was 5.2 mm/d with a mean precipitation of 2.8 mm/d. The 10 cm layer WC is strongly affected by water inputs, but also decayed at a higher rate than the 35 cm layer that slowly drops throughout the experiment. Evapotranspiration increased as the weather warms, but shows a clear drop at the beginning of the second experiment (figure 3.4). For the latter, irrigation and grass cut induced a decrease of mean daily ET to 4.7 mm/d and mean water supply to 2.1 mm/d.

In the case of L1, mean daily ET during the first experiment reached 5.6 mm/d with a mean precipitation

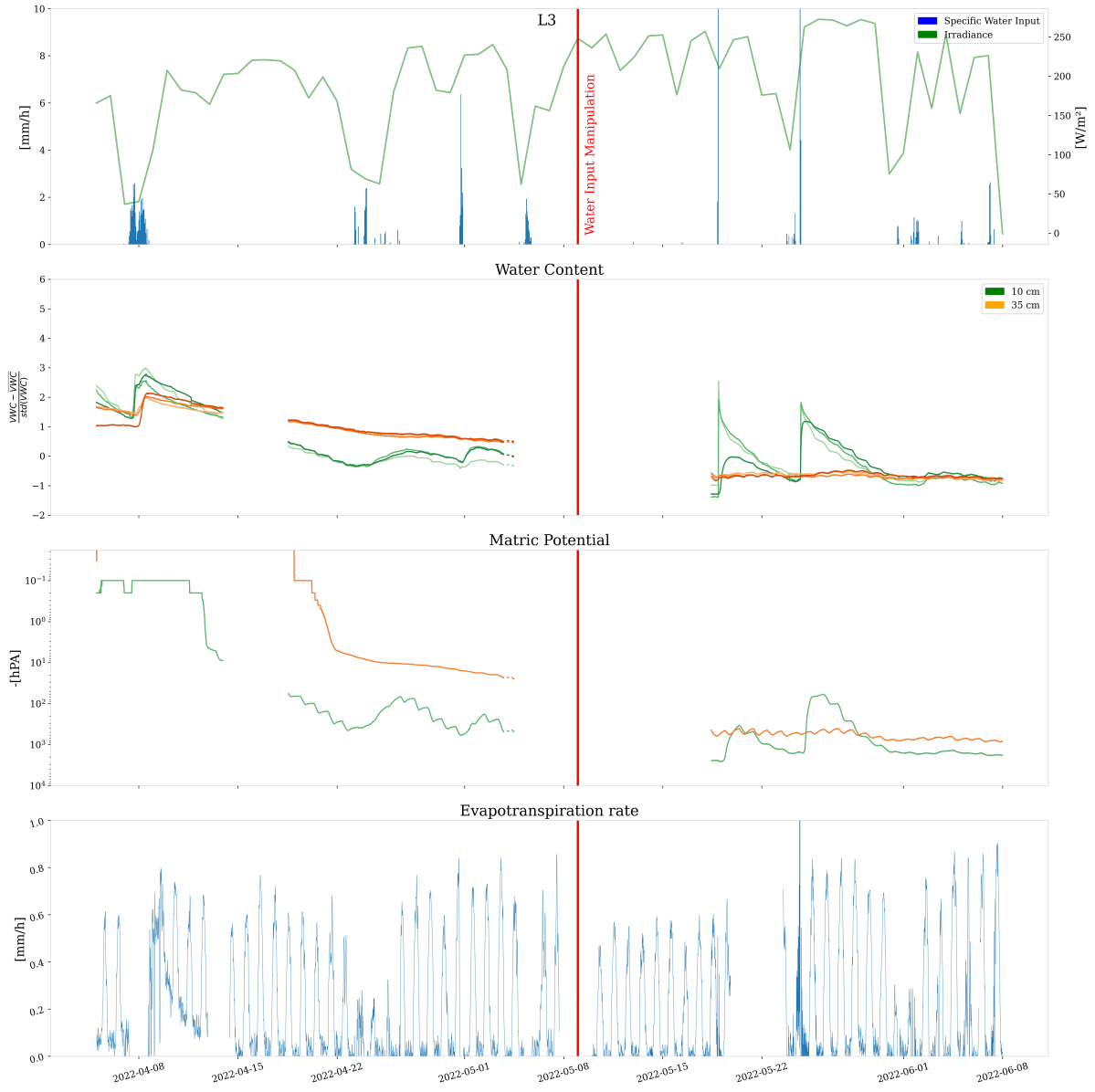

Figure 3.4: Summary of data for L3

value of 2.8 mm/d. Similarly to L3, the 35 cm layer WC is more stable than at 10 cm. As pointed out in other lysimeters, the grass cut at the beginning of the second experiment followed by dry conditions decreased mean daily ET to 3.6 mm/d and precipitation were null due to sheltering.
Figure **??** shows that the daily ET rate dynamics as fundamentally different between the vegetated lysimeters (L6, L3, L1) and bare soil. The precipitation event on the night between the 30th of April and the 1st of May resulted in a much greater relative increase for the latter, then rapidly decreased back to its previous value. Conversely, vegetated lysimeters decreased progressively over the following days.

Soil water follow very similar patter for vegetated lysimeters, in particular, L3 and L1 during the natural conditions experiment (figures 4.4 and 3.6). The bare soil lysimeter (L4) is characterised by a weaker dampening effect of precipitation impulses, significant daily variations and high loss rate, that results in more homogeneous dynamics throughout the entire soil column than vegetated soils. WC responses at 35 cm deep to rain events in L6 are heavily damped. In particular, the increase on the 8_{th} of April follows a

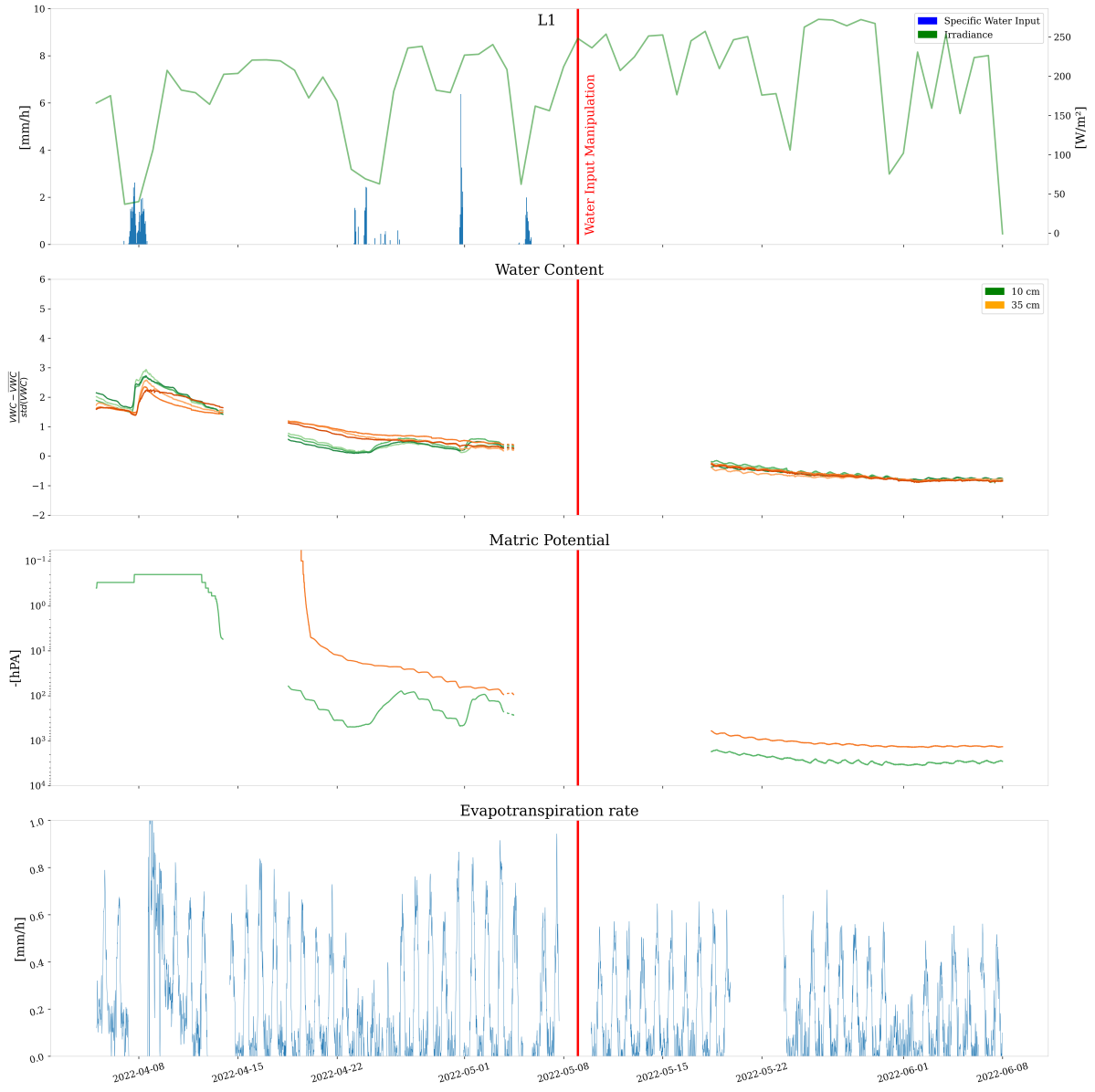

Figure 3.5: Summary of data for L1

saturation pattern, which may indicate that mean porosity of this layer is close to 30%. Irrigation applied during stress period on L6, L4 and L3 generated a more intense peak than naturally occurring rain events. At 10 cm depth, L4 and L3 decrease close to their original state after approximately a week and stabilise close to mean value, whereas L6 keeps shifting down at both 10 and 35 cm depths.

Figure 3.7 highlight the shift in ET rate with L1 and L6 sheltered from natural water inputs.

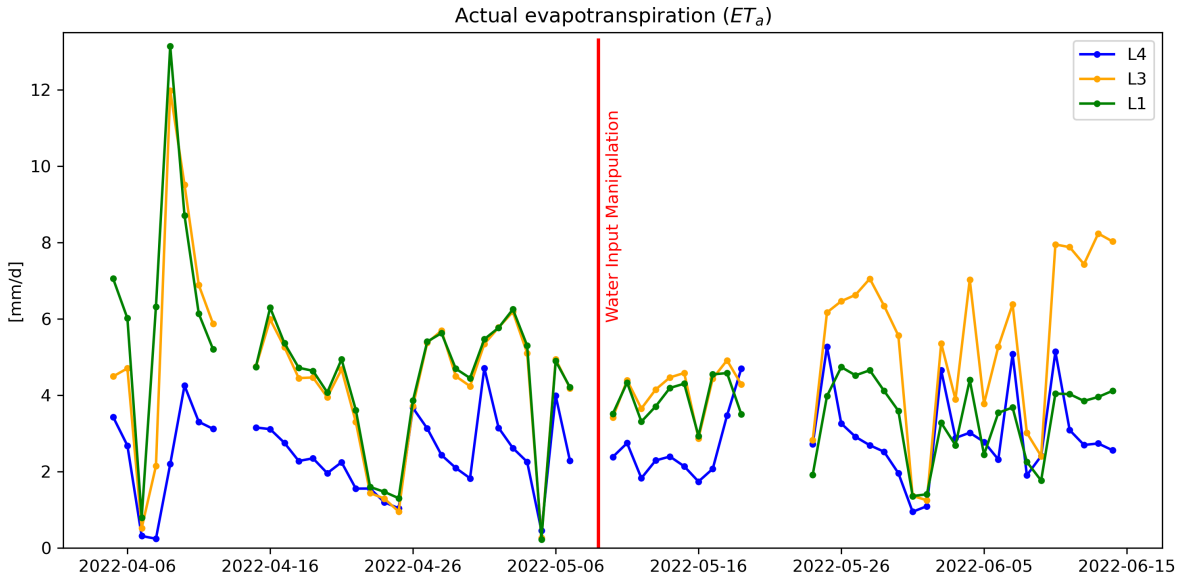

Figure 3.6: Measured daily ET. L6 displayed random drift patterns that limit our ability to draw coherent conclusions. They were removed for better readability.

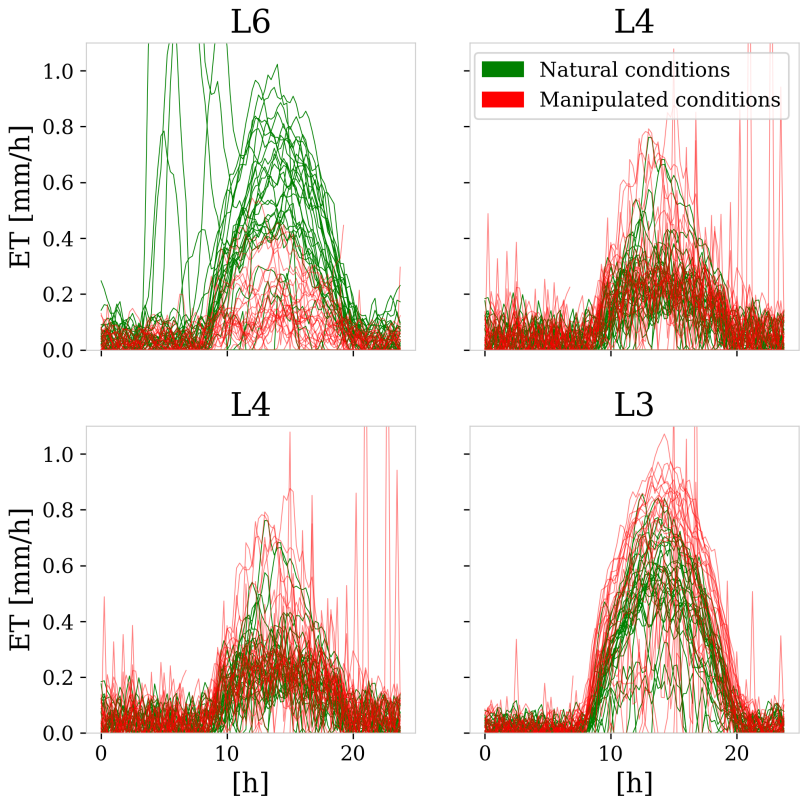

Figure 3.7: Evolution of 15 min ET during experiments. Color coding emphasizes the shift observed during water supply manipulation phase.

3.3 DATA GAPS

Discontinuities on plots presented in this report accounts for missing time interval. Manipulation errors during sensor network management and lack of consistency for maintenance lead to several loss of data both for the weight sensors and soil measurements. Moreover, the grass cutting were removed as such interventions generates meaningless weight variations

CHAPTER 4

DISCUSSION

4.1 EFFECT OF GRASS COVER ON EVAPOTRANSPIRATION

Evapotranspiration in the bare soil control lysimeter (L4) only accounts for the direct soil evaporation and provides a way to deduce the transpiration occurring in vegetated lysimeters. Comparison of mean fluxes of L1,L3 and L4 under standard conditions shows both fluxes have approximately the same magnitude. Consequently, the presence of grass doubles the evapotranspiration flux with respect to the latter.

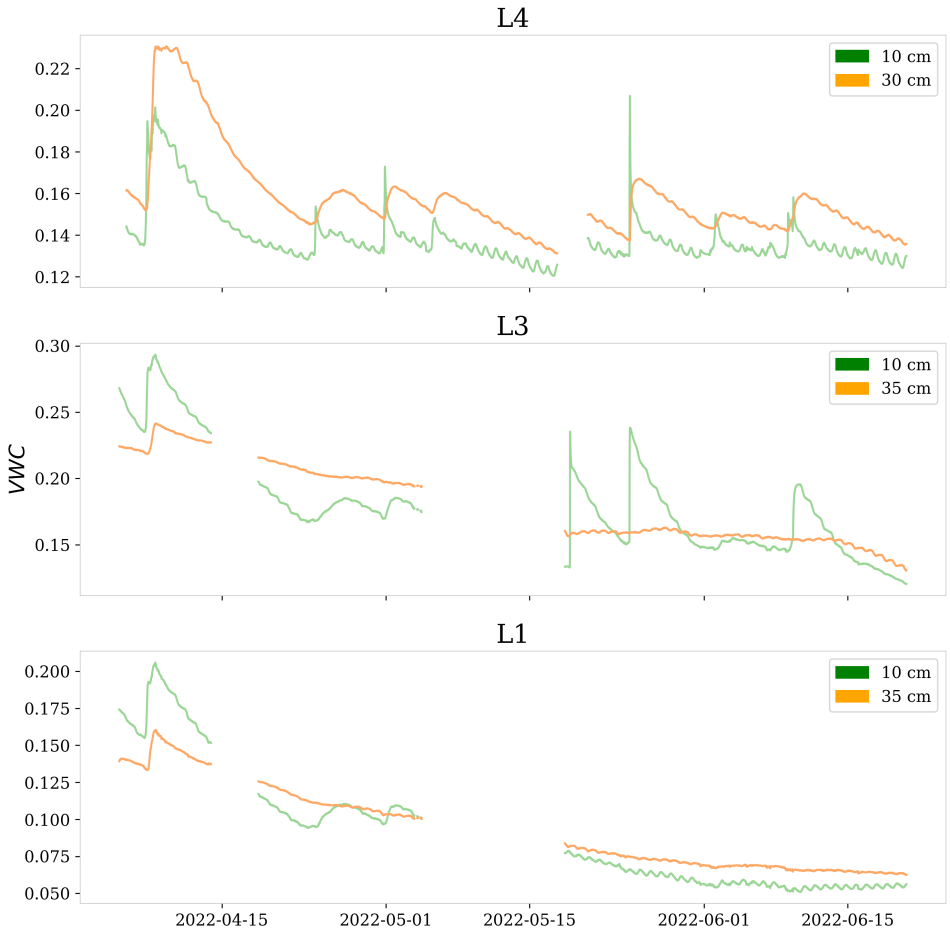

Figure 4.1: Comparison of VWC vertical dynamic between L1, L3 and L4. The green curve exceeding the orange one signifies that an upward gradient of water content forms in the soil column.

However, vegetation transpiration is heavily impaired by rain events and L4 ET rate decreases less than in L6, L4, L3 such that it tends to be higher on these particular periods (figure 3.6). As the weather clears over the following days, daily bare soil ET rapidly decreases (L4), whereas vegetated soil follows an opposite pattern as shown in figures 4.2. This supports the hypothesis that ET increases in bare soil because of the high availability of water in shallow layers until it infiltrates further down. On the contrary, vegetation is able to maintain the water available over several days and transpires at controlled rate. In addition, water tension values reached in L1, L3 and L6 compared to L4 (figure 3.6) and show the great suction applied by roots to extract moisture form the soil. This demonstrates the great ability of vegetation to increase water availability and optimise the withdrawal rate to sustainably manage storage.

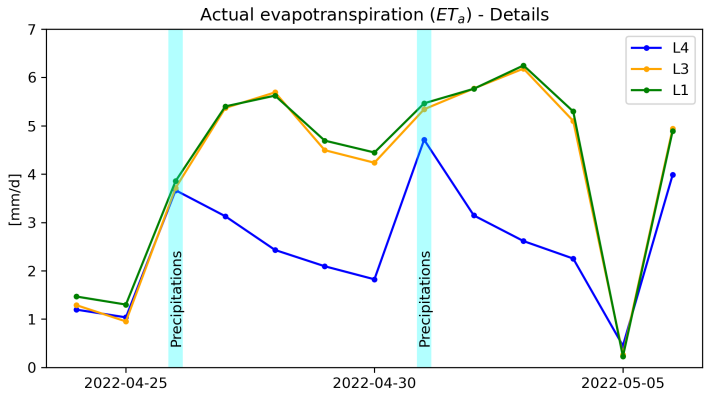

Figure 4.2: Highlight on the respond opposite behavior to a rain event between vegetated lysimeter and the bare soil during the natural conditions experiment.

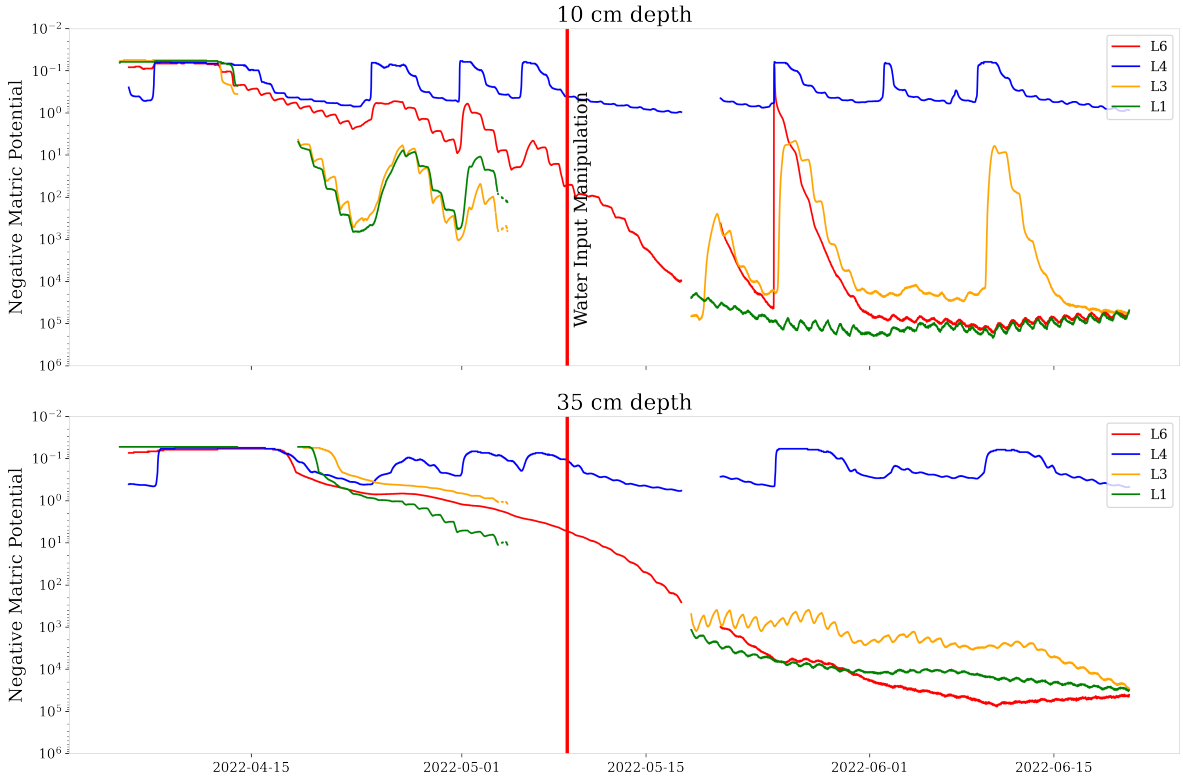

Figure 4.3: Matric potential comparison between lysimeters. The logarithmic negative values are displayed on an inverted axis. An upward curve corresponds to an increase of water availability

The surface of the bare soil lysimeter became more and more sealed. During rain events, water erodes the soil particles and carries them in the surface openings. As the fine portion of particles settles slower they tend to seal the surface and limit the penetration rate of water (figure 4.6). As the root network of vegetation develops, it structures the soil layers and modifies the distribution of water and nutrients and prevents the sealing of the surface. When water enters the top of a soil column it slowly travels downward and diffuses both horizontally and vertically. L4 WC curve details (figure **??**) shows the effect of the infiltration of rain in the soil column with a lag of 2 days between the two depths and a defined peak at 10

cm depth that smoothed out over 4 days at 30 cm. Grass cover reinforce this pattern by strongly reducing the downward flux of water. As a result, the 35 cm curve of L3 in figure 4.4 only reacts to the prolonged precipitation event between the 7^{th} and the 8^{th} of April (3.1).

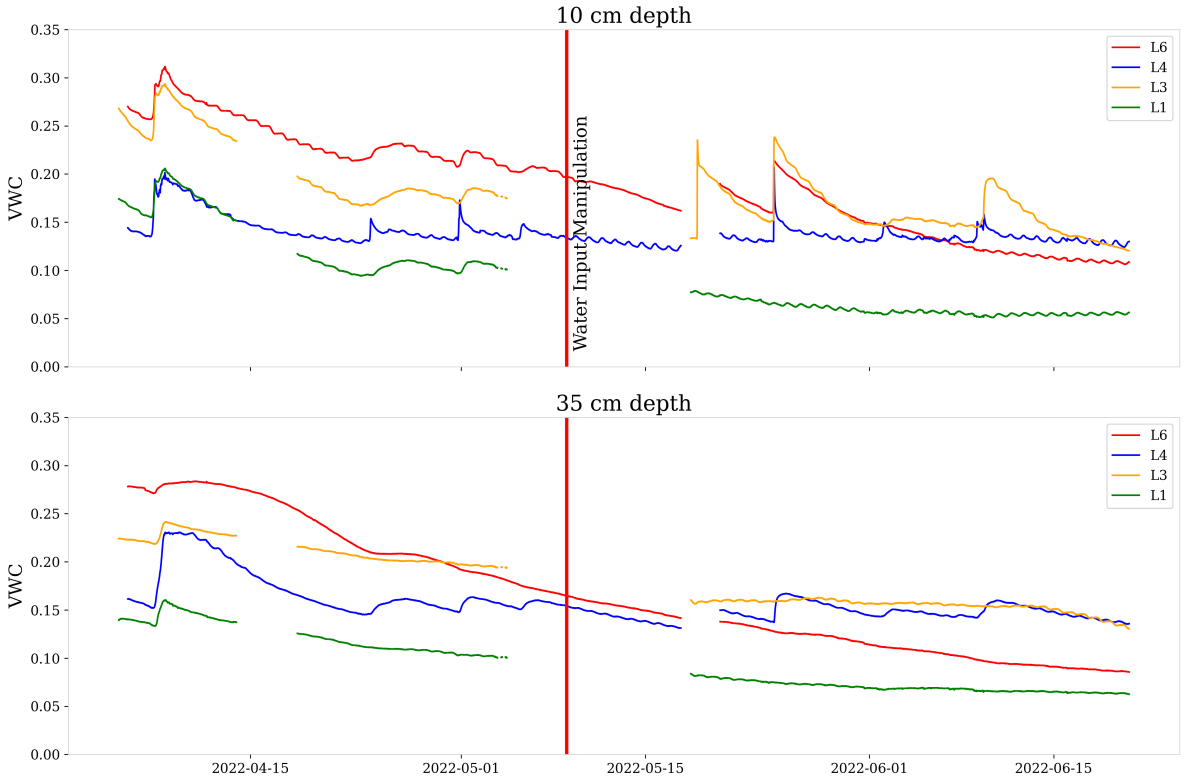

Figure 4.4: Water content comparison between lysimeters. As described in chapter 2.2.3, L4 probes were installed at 10 and 30 cm.

Water management strategy of vegetation significantly alters vertical water exchanges and modifies the storage depth distribution. Figure 4.1 indicates that in bare soil (L4) water mostly accumulates in deeper soil layers. During rain events, water rapidly infiltrates to the 30 cm layer. This flux rapidly builds up a downward gradient from the end of rain events. Furthermore, this implies that the ability of water to move from deep layers to the surface by capillarity limits water availability for ET. In contrast, vegetation confines water in the root zone and L3 deeper layer receives a very limited amount of water during the intense raining on the 7_{th} of April. Similarly, WC fast decay at root depth demonstrates that grass absorbs soil moisture very efficiently as the water availability suddenly increases at root depth from surface input. This supports the hypothesis that in high WC conditions, vegetation limits the leakage from root zone to deeper soil layers and ultimately increases water availability.

Figure 4.6: Localised surface accumulation during dripping irrigation of the bare soil.

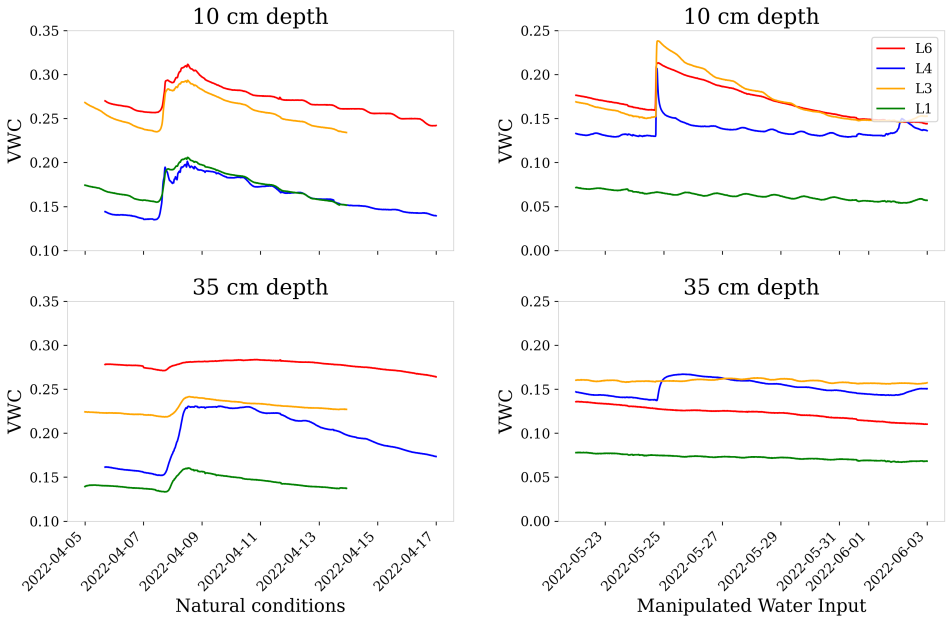

Figure 4.5: Detailed comparison between lysimeters of the diffusion pattern of a water input at 10 and 35cm depths during standard and stress conditions. The y axis ranges have the same difference to highlight the similarity of amplitudes.

4.2 EFFECT OF DROUGHT ON VEGETATION TRANSPIRATION

As lack of precipitation extends over long periods, water becomes more and more scarce in the root zone and forces vegetation to adapt its behavior. While L4 WC is barely impaired by the drought during the second experiment, L3 shallow layer moisture lower value is clearly bounded by deeper layers. In addition, stress conditions of vegetation in L1 are characterised by similar WC values across the soil column. The shift from the high vertical variability of water content during wet conditions to the quasi homogeneous dynamics on the soil column proposes that grass preferentially exploits water close from the surface but increases the withdrawal depths as water becomes scarce. Figure 3.6 shows that while the mean ET rate of L1 in stress condition during the second experiment is much smaller than L3, they both follow a similar dynamic. However, the $ET_a/ET_{potential}$ ratio during June for L3 remains constant in figure 4.7 which is consistent with the clear increasing tendency of actual ET.

When shallow soil water evaporates during droughts, moisture distribution across the soil column shifts far from its equilibrium state during balanced weather conditions. As described in chapter 4.1, vegetation withdraws shallow water very efficiently such that the root suction confines small water impulses in the root zone. This phenomenon intensifies as water becomes scarce. Irrigation in vegetated lysimeters (L3, L6) under drought conditions (18^{th}, 24^{th} of May) induced a significant drop of water tension and increase of WC at 10 cm, followed by rapid increase back to their initial values (figure 4.3 and 4.4). The bare soil (L4) follows a similar pattern but with a much smaller variation, whereas the deeper layers of L3 remain almost unaffected with respect to L4. This shows the little implications of deep water storage for ET process following precipitations in dry conditions.

The Penman Monteith FAO model establishes that potential evapotranspiration increases during summer due to more intense solar radiations and higher air temperature. However, without regular water input (precipitation, infiltration, irrigation,...) droughts can rapidly generate intense stress conditions as

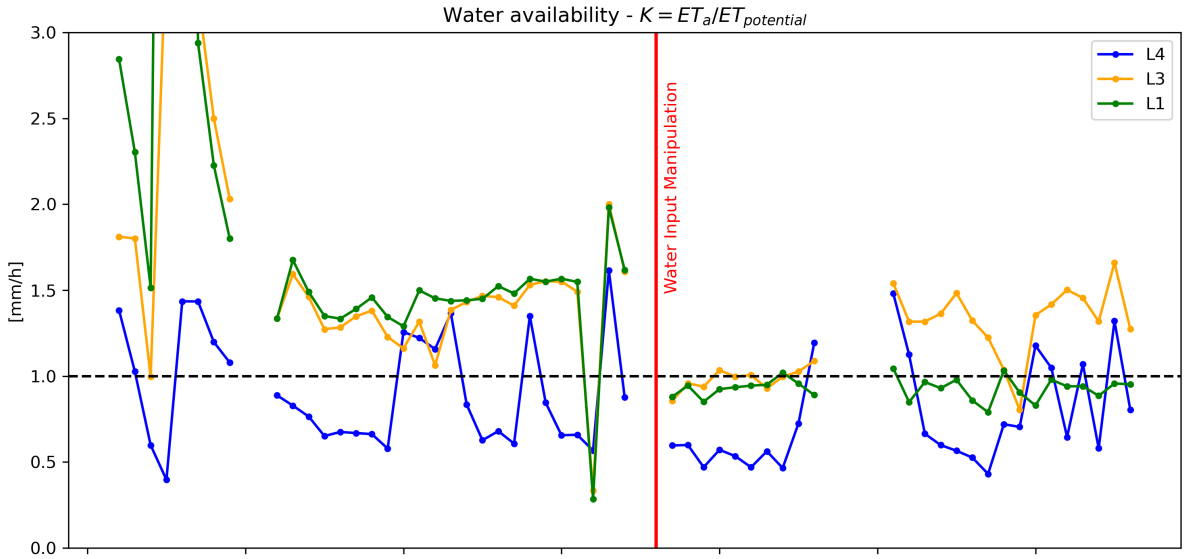

Figure 4.7: Fraction of actual ET over the potential ET according to the Penman Monteith FAO estimation method. The generalised exceeding of 1.0 value of the availability factor points toward a net under estimation of $ET_{potential}$ and is only used to put ET_a in perspective of variable atmospheric conditions

water availability drops and endangers vegetation survival. Typically, leaves start withering and might irreversibly brown. During experiment, lysimeters L1 and L3 exceeded 10 mm/d after the rain even in the beginning of April (figure 3.1). Figure 4.7 shows that the potential ET computation using Penman-Monteith FAO method does not reproduce the behavior and largely underestimates the subsequent actual ET.

In contrast, the $ET_{potential}$ gives a very good estimation for the beginning of the second experiment. Comparison of figure 3.6 and 4.7 demonstrates that the increase of potential ET reduction is the main driver of the $ET_{real}/ET_{potential}$ ratio drop rather than ET in L1 and L3. This suggests that the cutting of grass on the 9^{th} of May heavily impaired its transpiration ability. The drought conditions imposed to L1 limited the regrowth of vegetation whereas grass density recovered rapidly in L3. Two weeks after this manipulation, the $ET_{real}/ET_{potential}$ ratio of L1 does not present major change. In contrast, L3 increase to reach similar values than during the first experiment. Moreover, soil water content is generally lower during June and can not explain the increase of ET rate. These patterns demonstrate that water scarcity and vegetation in poor conditions severely limit the actual evapotranspiration rate (ET_a).

CHAPTER 5

CONCLUSION

This project involved the experimental collection of evapotranspiration data through the monitoring of weight variations in vegetated lysimeters. In parallel, an autonomous soil sensor network that monitors water tension and soil moisture provides an estimate of water availability. The analysis of the collected data leads to the following conclusions:

- Vegetation roots apply a great suction effect to the soil to withdraw water. As a result, the water tension at root level increases significantly and limits the leakage to deeper soil layers. Furthermore, vegetation has an important buffering effect on water inputs. As soil water content peaks, the transpiration rate progressively increases over several days which shows the vegetation aptitude for sustainable water resources management. Overall, vegetation substantially increases the water availability for evapotranspiration; in balanced atmospheric and soil moisture conditions, grass covered soil evapotranspirates twice as much water as a bare soil.
- Vegetation preferentially exploits water close to the surface, but extends its withdrawal depth during droughts. Under these conditions, water withdraw becomes highly efficient and even large water inputs are rapidly and fully recovered by the roots intense suction. As vegetation optimises its behaviour to survive, water exchanges across the soil column become almost null. The $ET_a/ET_{potential}$ ratio follows complex dynamics in stress conditions and is particularly impaired as vegetation approaches its wilting point.

Finally, the data acquired from the monitoring of evapotranspiration in vegetated lysimeters allowed to highlight important patterns that intervene in the response of water availability to droughts. These results motivate the need of further exploration of the provided data set and suggests that accurate measurements of evapotranspiration and vegetation-soil interactions are fundamental to develop our understanding of water availability dynamics.

BIBLIOGRAPHY

Benettin, Paolo et al. (2021). 'Tracing and Closing the Water Balance in a Vegetated Lysimeter'. en. In: *Water Resources Research* 57.4. _eprint: https://onlinelibrary.wiley.com/doi/pdf/10.1029/2020WR029049, e2020WR029049. ISSN: 1944-7973. DOI: 10.1029/2020WR029049. URL: https://onlinelibrary.wiley.com/doi/abs/10.1029/2020WR029049 (visited on 7th June 2022).

Queloz, Pierre et al. (Apr. 2015). 'Transport of fluorobenzoate tracers in a vegetated hydrologic control volume: 1. Experimental results'. en. In: *Water Resources Research* 51.4, pp. 2773–2792. ISSN: 0043-1397, 1944-7973. DOI: 10.1002/2014WR016433. URL: https://onlinelibrary.wiley.com/doi/abs/10.1002/2014WR016433 (visited on 26th June 2022).

Fatichi, Simone, Christoforos Pappas and Valeriy Y. Ivanov (2016). 'Modeling plant–water interactions: an ecohydrological overview from the cell to the global scale'. en. In: *WIREs Water* 3.3. _eprint: https://onlinelibrary.wiley.com/doi/pdf/10.1002/wat2.1125, pp. 327–368. ISSN: 2049-1948. DOI: 10.1002/wat2.1125. URL: https://onlinelibrary.wiley.com/doi/abs/10.1002/wat2.1125 (visited on 29th May 2022).

Queloz, Pierre Claude Jean (2015). 'Experiments in hydrologic solute transport'. en. PhD thesis.

Topp, G. C., J. L. Davis and A. P. Annan (1980). 'Electromagnetic determination of soil water content: Measurements in coaxial transmission lines'. en. In: *Water Resources Research* 16.3. _eprint: https://onlinelibrary.wiley.com/doi/pdf/10.1029/WR016i003p00574, pp. 574–582. ISSN: 1944-7973. DOI: 10.1029/WR016i003p00574. URL: https://onlinelibrary.wiley.com/doi/abs/10.1029/WR016i003p00574 (visited on 21st June 2022).

Colin Campbell, C. Chambers (2016). *Campbell Scientific example programs*.

APPENDIX A

APPENDIX

A.1 DETAILS ON LYSIMETERS WEIGHT SENSOR NETWORK PARTS

(a) Junction box, VKK1-4, HBM

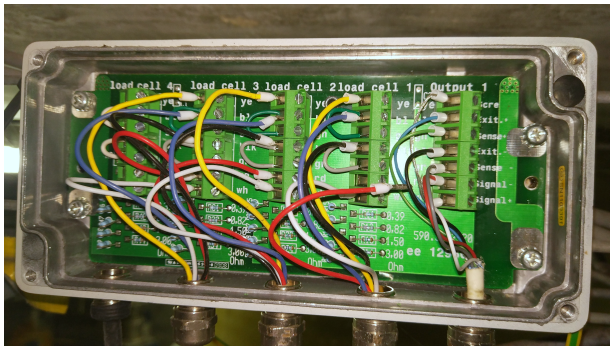

(b) Analog to digital transducer, AED9201B, HBM

A.2 Details on grass installation

A.3 Details on soil sensor installation

Figure A.3: Detailed procedure for 5TM water content sensor and TEROS 21 tensiometer installation

Figure A.4: Clod of grass extracted during the sensor installation